中国光学（中英文） Chinese Optics 核心期刊

Study of bonding layer for integrated structure of space gravitational wave detector telescope

ZHAO Hong-chao, LIU Chang, ZHOU Wen-ke, ZHU Han-bin, CHEN Wen-duo

Citation:
ZHAO Hong-chao, LIU Chang, ZHOU Wen-ke, ZHU Han-bin, CHEN Wen-duo. Study of bonding layer for integrated structure of space gravitational wave detector telescope[J]. *Chinese Optics*, In press. doi: 10.37188/CO.EN-2024-0025
赵宏超, 刘畅, 周文科, 朱汉斌, 陈文多. 空间引力波探测望远镜集成结构的胶接方法研究[J]. 中国光学, 优先发表. doi: 10.37188/CO.EN-2024-0025

View online: https://doi.org/10.37188/CO.EN-2024-0025

文章编号　2097-1842(xxxx)x-0001-10

Study of bonding layer for integrated structure of space gravitational wave detector telescope

ZHAO Hong-chao[1], LIU Chang[2], ZHOU Wen-ke[1], ZHU Han-bin[1], CHEN Wen-duo[3*]

(1. *School of Advanced Manufacturing*, *Shenzhen Campus of Sun Yat-sen University*, *No. 66*, *Gongchang Road*, *Guangming District*, *Shenzhen*, *Guangdong* 518107, *P.R. China*;

2. *School of Aeronautics and Astronautics*, *Sun Yat-Sen University*, *No. 66*, *Gongchang Road*, *Guangming District*, *Shenzhen*, *Guangdong* 518107, *P.R. China*;

3. *School of Materials*, *Shenzhen Campus of Sun Yat-sen University*, *No. 66*, *Gongchang Road*, *Guangming District*, *Shenzhen*, *Guangdong* 518107, *P.R. China*)

* *Corresponding author*, *E-mail*: *chenwd*29@*mail.sysu.edu.cn*

Abstract: To detect gravitational waves in space, the telescope and optical platform require high stability and reliability. However, the cantilevered design presents challenges, especially in the glass-metal hetero-bonding process. This study focuses on the analysis and experimental research of the bonding layer in the integrated structure. By optimizing the structural configuration and selecting suitable bonding processes, the reliability of the telescope system is enhanced. The research indicates that the use of J-133 adhesive achieves the best performance, with a bonding layer thickness of 0.30 mm and a metal substrate surface roughness of Ra 0.8. These findings significantly enhance the reliability of the optical system while minimizing potential risks.

Key words: space gravitational-wave detector; integrated structure; glass-metal hetero-bonding

收稿日期:2024-07-31; **修订日期**:2024-09-04

基金项目:深圳市高等院校稳定支持计划 (No. 20220818153519003); 国家重点研发计划(2021YFC2202103); 国家自然科学基金项目(No. 22341303)

Supported by Shenzhen Science and Technology Program (No. 20220818153519003); National Key R & D Program of China (No. 2021YFC2202103); National Natural Science Foundation of China (No. 22341303)

空间引力波探测望远镜集成结构的胶接方法研究

赵宏超[1], 刘　畅[2], 周文科[1], 朱汉斌[1], 陈文多[3*]
（1. 中山大学 先进制造学院, 广东 深圳 518107;
2. 中山大学 航空航天学院, 广东 深圳 518107;
3. 中山大学 材料学院, 广东 深圳 518107）

摘要: 为了实现超低频段空间引力波的探测, 望远镜和光学平台的集成结构需要具有极高的稳定性和可靠性。然而, 望远镜悬臂梁式的设计对集成结构的研制提出了重大挑战, 特别是依赖于玻璃-金属异质键合的粘接结构。为了应对这些挑战实现望远镜系统的高可靠性研制, 本研究对集成结构粘合层进行了设计、分析和实验研究。研究表明, J-133 粘合剂在粘接层厚度为 0.30 mm、金属基板的表面粗糙度为 Ra 0.8 时具有最佳性能。这些发现显著提高了光学系统的可靠性, 同时最大限度地降低了潜在风险。

关　键　词: 空间引力波探测器; 集成结构; 玻璃-金属异质键合
中图分类号: O348　　**文献标志码:** A　　**doi:** 10.37188/CO.EN-2024-0025　　**CSTR:** 32171.14.CO.EN-2024-0025

1 Introduction

The advancement of gravitational wave detection has led to projects dedicated to detecting gravitational waves in the 0.1 mHz~1 Hz range using intersatellite laser interferometry[1-3]. These projects plan to use the triangular formation of three identical drag-free satellites as a space observatory to achieve this goal. Each satellite carries two sets of core payloads, i.e., movable optical subassemblies (MOSAs), to construct intersatellite laser interferometric links over a baseline of 0.17–3 billion km. To detect gravitational-wave signals in space, the laser interferometric measurement system must achieve an optical path stability level than 12 pm/Hz$^{1/2}$@ 0.1 mHz~1 Hz, which imposes stringent requirements on the stability of the laser interferometric measurement system[4-6].

As a critical optical system for laser transmission and reception, any minute disturbance within the telescope will couple into optical path changes, significantly impacting the measurements. To achieve the required stability in performance, an all-zero-dur off-axis four-mirror telescope is proposed that utilizes materials with ultralow thermal expansion coefficients to reduce the optical path stability noise introduced by the telescope. Although this approach enhances the stability of the telescope, it also presents significant challenges in the structural design. On one hand, the brittle nature of the crystal material results in a noticeable increase in the telescope's mass. On the other hand, it complicates the integration of the telescope with the optical platform.

To address these challenges, this study conducted simulation and experimental research on the design of integrated structures, especially the bonds, to develop an integrated structure with outstanding reliability.

2 Integrated structure and bonding layer analysis

Traditionally, flexible structures have been preferred as the optimal solution for space applications[7]. Flexible structures can effectively reduce internal stresses and ensure the stability of payload positions by decoupling the degrees-of-freedom. Flexible structures can also isolate vibrations and thermal loads, thereby reducing the response of the payload to forces and thermal fluctuations. However, in space gravitational-wave detection systems,

where the ultrahigh stability of the payload is paramount, spacecraft have disabled all movable mechanisms and instead employed a multilevel thermal control system to achieve exceptionally high internal temperature stability[8-9]. To meet the measurement goal of 12 pm/Hz$^{1/2}$@0.1 mHz~1 Hz, the integrated structure must possess characteristics of kinematic support. This allows the assessment of misalignments between the telescope and optical axis of the interferometer by monitoring the thermal loads. The design of the integrated structure is shown in Fig. 1(a).

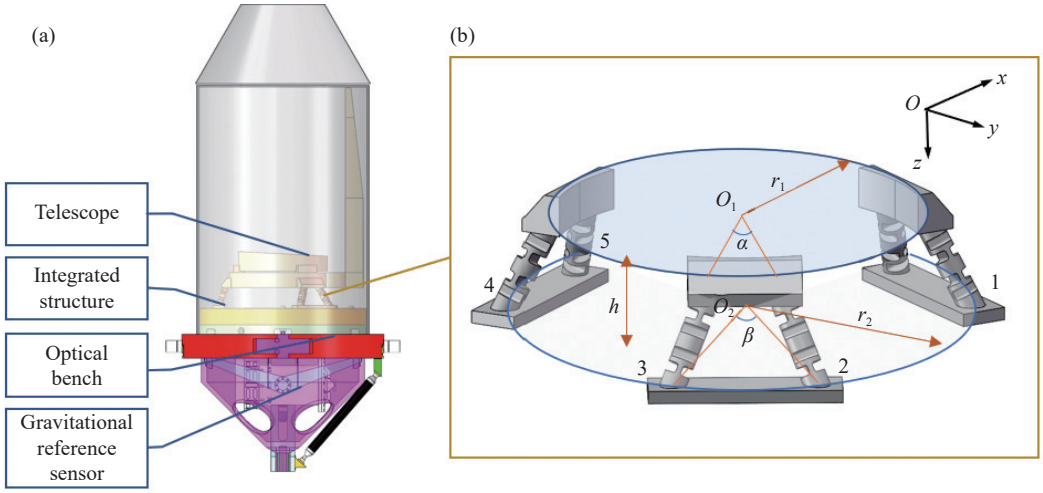

Fig. 1 Movable optical subassemblies (MOSAs) and integrated structure. (a) Key components of movable optical subassemblies and (b) integrated structure and design parameters.

2.1 Integrated structure design

The integrated structure consisted of three sets of bipod flexible supports. The overall structure was the same as that of a six degrees-of-freedom parallel structure. This structure features high forward stiffness, strong load-bearing capacity, and accurate positioning, effectively reducing the coupling between the degrees-of-freedom. The integrated structure adopts a radial three-point support scheme. In terms of design, to ensure the rigidity of the integrated structure, it is generally required that the rigid planes of the three sets of bipods pass through the telescope's center of mass. Therefore, apart from the flexible joints, the design parameters mainly consist of four physical parameters: the upper support radii r_1, lower ring support radii r_2, angle between the upper support points α, and angle between the lower support points β, as shown in Fig. 1(b).

The aforementioned integrated structure was used as the research object. Using the flexible rod axial force and first-order modal frequency as optimization objectives, a multi-objective optimization method was employed to optimize the parameters of the integrated structure. The optimization results are listed in Table 1.

Tab. 1 Optimal solution of integrated structural parameters.

Variables	Range of values	Optimization results
The upper ring support radii r_1/mm	150–180	180.0
The lower ring support radii r_2/mm	180–240	206.5
The angle between the upper support points α/°	5–20	15.7
The angle between the lower support points β/°	15–40	35.0

A detailed modeling of the integrated design with the telescope system was conducted, followed by a modal analysis to verify the feasibility of the existing design. The analysis results indicated that the integrated structure with the overall telescope system could reach a first-order resonance frequency of 147 Hz. The second- and third-order mode shapes were all related to the integrated structure, vibrating in the x- and y-directions with resonance frequencies of 207 Hz and 209 Hz, respectively, as shown in Fig. 2.

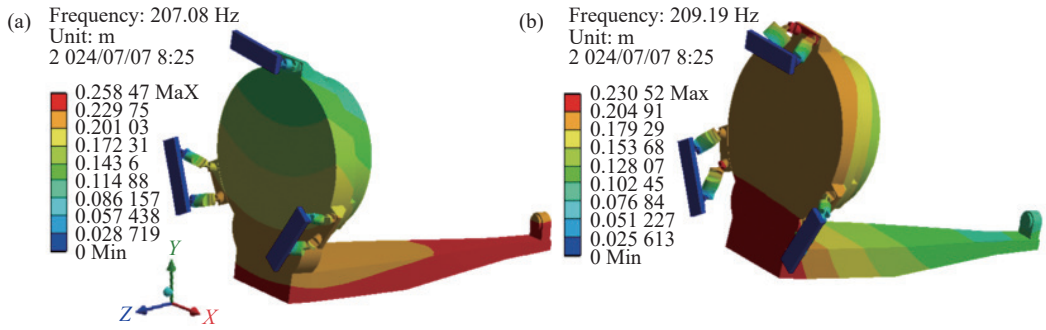

Fig. 2 The second and third modal shapes. (a) The second modal shape and (b) third modal shape.

2.2 Bonding simulation

The ultra-stable telescope and flexible support structure require the use of a reliable connection method for integration. The most commonly used solution to achieve a connection between different materials is glass-metal heterogeneous bonds, which can isolate and protect the optics from mechanical and thermal loads[10]. Owing to the more uniform distribution of shear stress, it is possible to effectively utilize the bonding area and enhance the bonding strength[11]. Therefore, a side-bonding structure is adopted for this design.

In the field of gravitational-wave detection, the most well-known bonding method is hydroxide-catalysis bonding[12-13]. However, this method cannot be applied to heterogeneous glass-metal bonding. Currently, suitable adhesives in the aerospace industry include epoxy resins, polyurethanes, and silicone. Owing to their various chemical compositions, they have different characteristics, functions, and applications. As a stiff bond, epoxy adhesives can maintain alignment and provide exceptional bonding strength while exhibiting minimal shrinkage. This unique characteristic makes them ideal for bonding materials with varying coefficients of thermal expansion, such as the bonding of metal and glass. Compared with epoxy resins, polyurethane adhesives have the advantage of low-temperature curing, providing improved toughness and low-temperature resistance. Silicone adhesives have relatively weaker bonding strengths, but offer advantages such as high- and low-temperature resistance, temperature variation resistance, and UV radiation resistance.

Considering the application attributes of various space adhesives and the bonding requirements of the ultra-stable telescope, the selection of space adhesives should prioritize those with higher bonding strength, stable performance, and convenient curing processes while meeting the basic principles of space applications. Epoxy adhesives, with their high tensile shear strength, reliable bonding performance, and mature processability, were chosen as the adhesive for the connection. Following a comprehensive investigation, three types of adhesives were selected as alternatives.

During the launch, the telescope was positioned horizontally[14]. A detailed simulation was conducted to examine the stress imposed on the bonding layer resulting from random vibrations, as shown in Fig. 3.

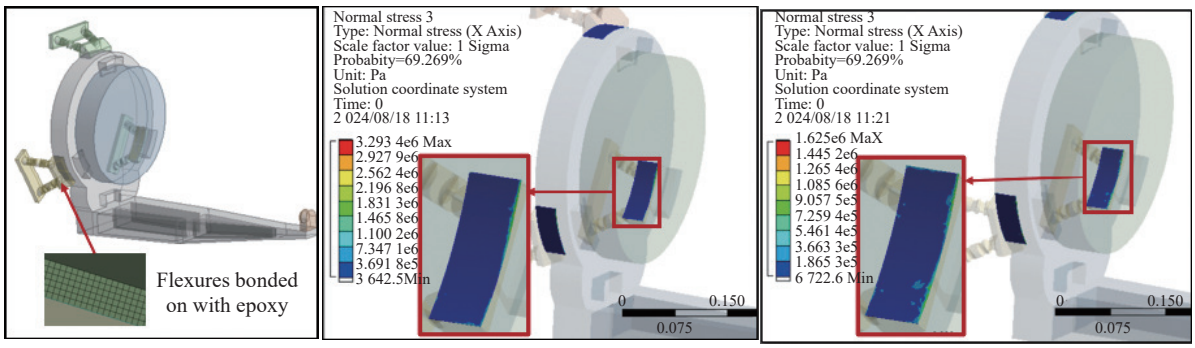

Frequency/Hz	PSD
20	0.001 g^2/Hz
40	0.01 g^2/Hz
500	0.01 g^2/Hz
700	0.02 g^2/Hz
1 200	0.02 g^2/Hz
2 000	0.004 g^2/Hz
Direction	X、Y、Z

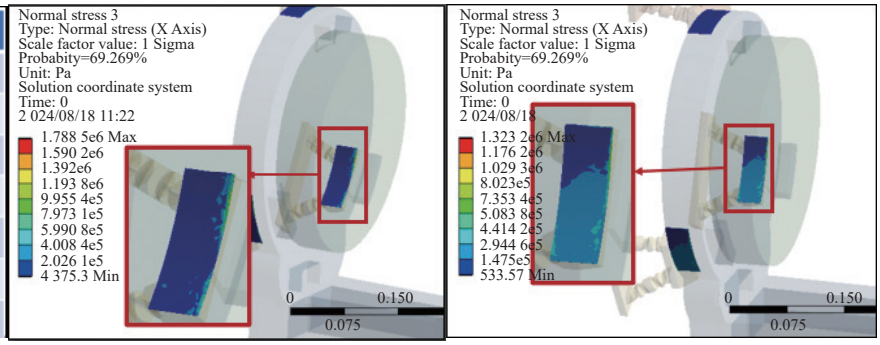

Fig. 3　Stress cloud map of bonding layer in random vibration analysis. (a) Flexures bonded on with epoxy. (b) Maximum normal stress cloud map when excitations are applied in the x-direction. (c) Maximum normal stress cloud map when excitations are applied in the y-direction. (d) Random vibration inputs. (e) Maximum normal stress cloud map when excitations are applied in the z-direction. (f) Maximum shear stress cloud map of the bonding layer.

It is evident that the bonding layer experienced both shear stress and normal stress, with the maximum normal stress reaching 3.29 MPa (1σ). Furthermore, owing to the influence of a diminished Poisson's ratio, the typical epoxy material experiences heightened stress at its edges, as shown in Fig. 3(c). Consequently, experimental investigations to ascertain the tensile strength of the bonding layer are of paramount importance.

3　Metal-glass bonding

3.1　Experimental design

Several factors influence the strength of adhesive bonds. Among these, the type of adhesive, bonding-layer thickness, and surface roughness are the main factors affecting the bond strength[15-16]. By comparing and selecting adhesives with excellent performance, conducting experimental tests and analysis can provide data support for estimating the structural strength, which is of practical significance for the integration of MOSAs in gravitational-wave detectors.

Generally, compared with a thicker bonding layer, a thinner bonding layer has a smaller stress concentration, and the bonding strength increases as the bonding-layer thickness decreases. This is because the increase in the bonding-layer thickness reduces the average stress in the thickness direction, leading to an increase in the peel moment and a decrease in strength. The optimal bonding-layer thickness for the structural bond is between 150–500 μm. However, the optimal thickness may vary depending on the type of adhesive, material, and application environment. Currently, the primary methods for determining the optimal bonding-layer thickness include empirical methods, heat dissipation formula calculations, and experimental comparisons[17-20]. This study adopts the experimental method to compare and select the most suitable bonding-layer thickness for the overall structure and flexible support for the gravitational-wave detector telescope. The candidate bonding-layer thicknesses was set as 0.15 mm, 0.30 mm, and 0.50 mm. The bonding-layer thickness is ensured by symmetrically placing fishing lines of the corresponding diameter on the bonding surface.

The surface condition of the adherend is another important factor affecting the performance. The adherend materials for the ultra-stable telescope bonding scheme were Invar steel and Zerodur. Therefore, using the same bonding process on Invar steel substrates with different surface roughness values resulted in different bonding strengths. According to the Wenzel wetting model for rough surfaces, the roughness factor r represents the ratio of the actual solid-liquid contact area to the apparent contact area, which leads to the Wenzel equation [21]:

$$\cos\theta_m = r\cos\theta_y \quad , \qquad (1)$$

where θ_m is the apparent contact angle on the rough surface and θ_y is the equilibrium contact angle of the liquid on an ideal surface.

According to this equation, it can be inferred that for hydrophilic surfaces, an increase in surface roughness increases the contact area between the solid and liquid, promoting the wetting action of the adhesive on the substrate surface and generating mechanical adhesion.

A controlled variable method was employed to investigate the influence of different variables on the overall bonding strength. Experimental research was conducted by comparing the performance of different adhesives at different thicknesses and substrate surface roughness. The experiment consisted of three groups, each containing 36 specimens, for a total of 108 specimens.

Tab. 2 Alternative epoxy adhesive and experimental design.

	Variables
Epoxy adhesive	J-133 GHJ-01(Z) 3M-DP2216
Bonding-layer thickness /mm	0.15 0.3 0.5
Surface roughness /μm	Ra0.8 Ra1.6 Ra3.2 Ra6.3
Single group specimens	36
Total specimens	108

3.2 Bonding process and tensile strength test

The substrates used for bonding consisted of two materials: Zerodur and Invar steel. The Zerodur component (Schott, Germany) is a flat mirror with a diameter of 50 mm and thickness of 10 mm. It features a highly polished surface with an RMS shape better than 1/30λ. The metal part was made of 4J36 Invar steel with a diameter of 20 mm and length of 30 mm. In addition, the surface roughness of the metal part was carefully controlled. In the bonding process, fishing lines of appropriate diameters were used to regulate the thickness of the bonding layer. To ensure reliable results, each bonding specimen with a singular controlled variable was subjected to three sets of control experiments, with each set comprising 36 specimens.

Prior to the bonding process, the substrates underwent a 16 h standing period in the laboratory. Strict measures were in place to maintain the coaxial alignment between the Invar steel test column and flat mirror. By employing fishing lines, a V-shaped positioning apparatus was carefully crafted on the bonding surface of the flat mirror, as shown in Fig. 4(a), effectively securing the desired thickness of the bonding layer. Following the completion of the bonding procedure, mechanical experiments were performed, giving the bonding layer sufficient time to achieve full bonding efficacy.

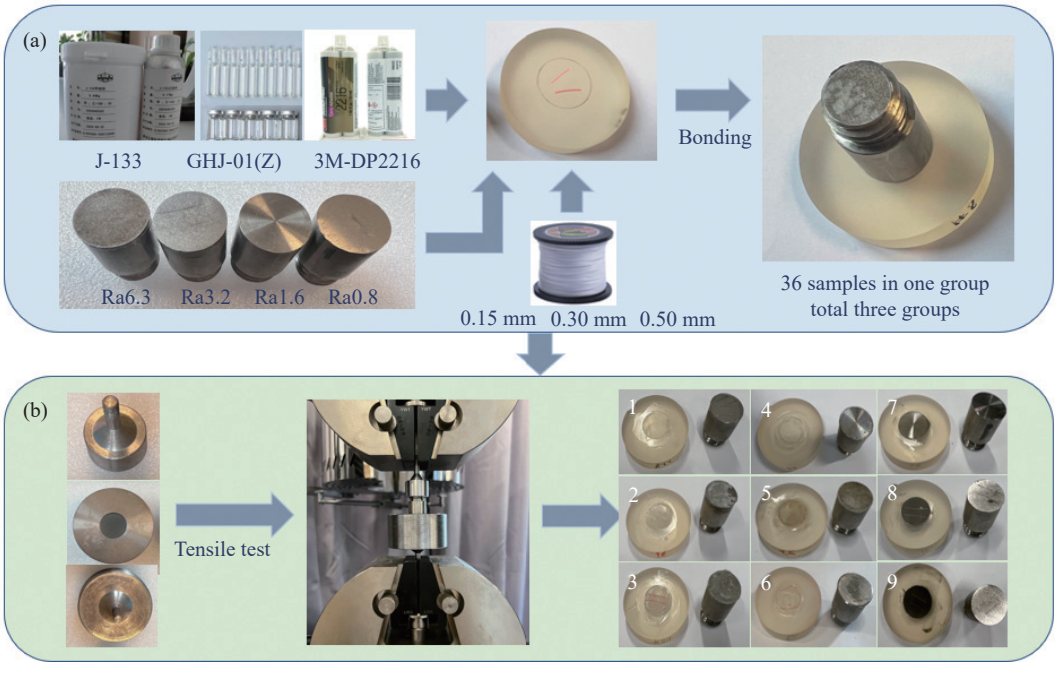

Fig. 4 Bonding process and tensile strength test. (a) Bonding process and (b) tensile strength test.

3.3 Test data

Utilizing the meticulously designed array of strength testing fixtures, the specimens were affixed onto the tensile testing machine to assess their tensile strength in accordance with established national testing standards. The configuration diagram detailing the testing process is shown in Fig. 4(b).

The test results for the J-133 adhesive underwent meticulous statistical analysis. As illustrated in Fig. 5(a), the specimens exhibited a notable range of tensile strengths from 12 to 22 MPa, primarily due to inherent variations in bonding-layer thickness and surface roughness. It was observed that there was a general declining trend in the tensile strength as the surface roughness of the substrate increased. The J-133 adhesive demonstrated its highest tensile strength when applied to a substrate with a surface roughness of Ra 0.8. Thus, it is clear that the bonding-layer thickness significantly influenced the tensile strength characteristics of the J-133 adhesive.

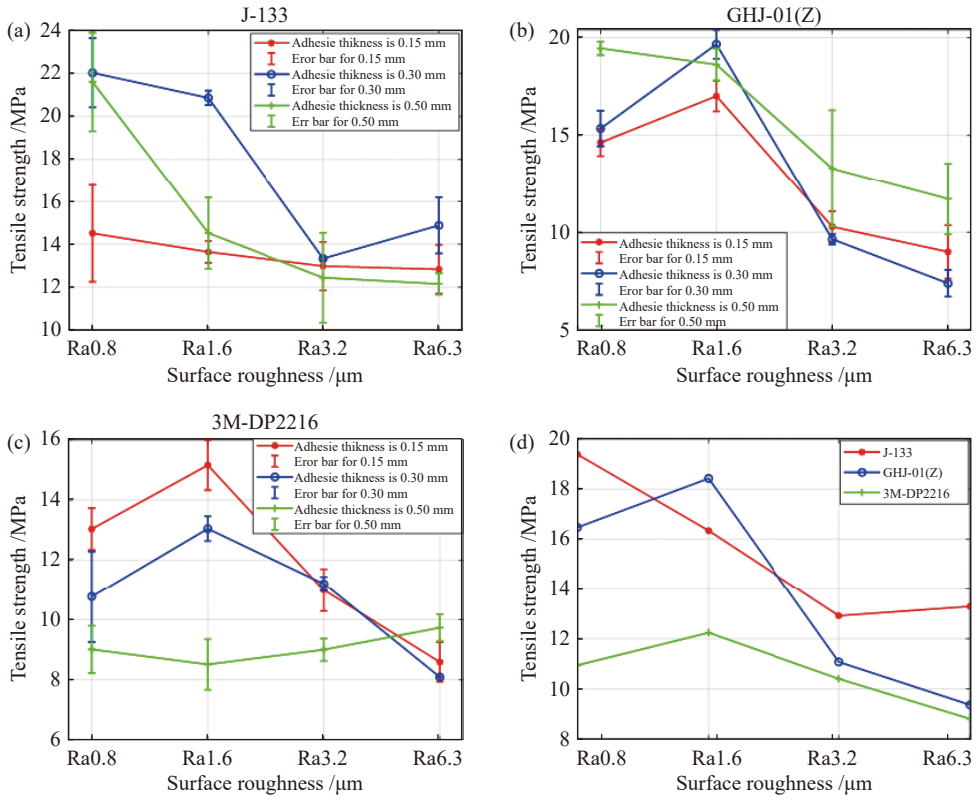

Fig. 5 Tensile strength test results. (a) Tensile strength test results of J-133 adhesive. (b) Tensile strength test results of GHJ-01(z) adhesive. (c) Tensile strength test results of 3M-DP2216 adhesive. (d) Average strength values of three adhesives at different roughness levels

Thorough statistical analysis was performed on the test results for the GHJ-01(Z) adhesive. In identical experimental conditions, the GHJ-01(Z) adhesive displayed a wide-range of tensile strengths from 7 to 20 MPa. As shown in Fig. 5(b), the GHJ-01(Z) adhesive exhibited exceptional performance when the substrate surface roughness was Ra 1.6, reflecting its optimal tensile strength and unwavering process stability.

A statistical analysis was conducted on the test results for the 3M-DP2216 adhesive. Compared with the previous two adhesives, the mechanical performance was slightly inferior, as shown in Fig. 5(c). However, when the bonding-layer thickness was set at 0.15 and 0.30 mm, most of the control groups still met the design requirements. Specifically, when the thickness was 0.15 mm and the substrate surface roughness was Ra 1.6, the 3M-DP2216 adhesive exhibited the best performance with a tensile strength of up to 15.16 MPa.

4 Results and discussion

The experimental analysis shows that the traditional acid-etching method for improving the adhesive performance is generally feasible during conventional bonding processes; however, excessive acid etching can lead to a decrease in adhesive performance. In addition, the bonding-layer thickness should be selected based on the performance of the adhesive itself, which was determined experimentally. The experimental results show that the J-133 adhesive has a significant advantage when the bonding-layer thickness is 0.30 mm and the substrate surface roughness is Ra 0.8, as shown in Fig. 5. The tensile strength exceeds 22 MPa, satisfying the strength requirements of the integrated structure of the telescope in the space gravitational-wave detector. Building upon this foundation, this section further analyzes the failure process of the bonding layer in tensile tests to enhance the reliability of the bonding.

Figure 6 illustrates the mechanism and process of the J-133 bonding-layer failure during tensile testing.

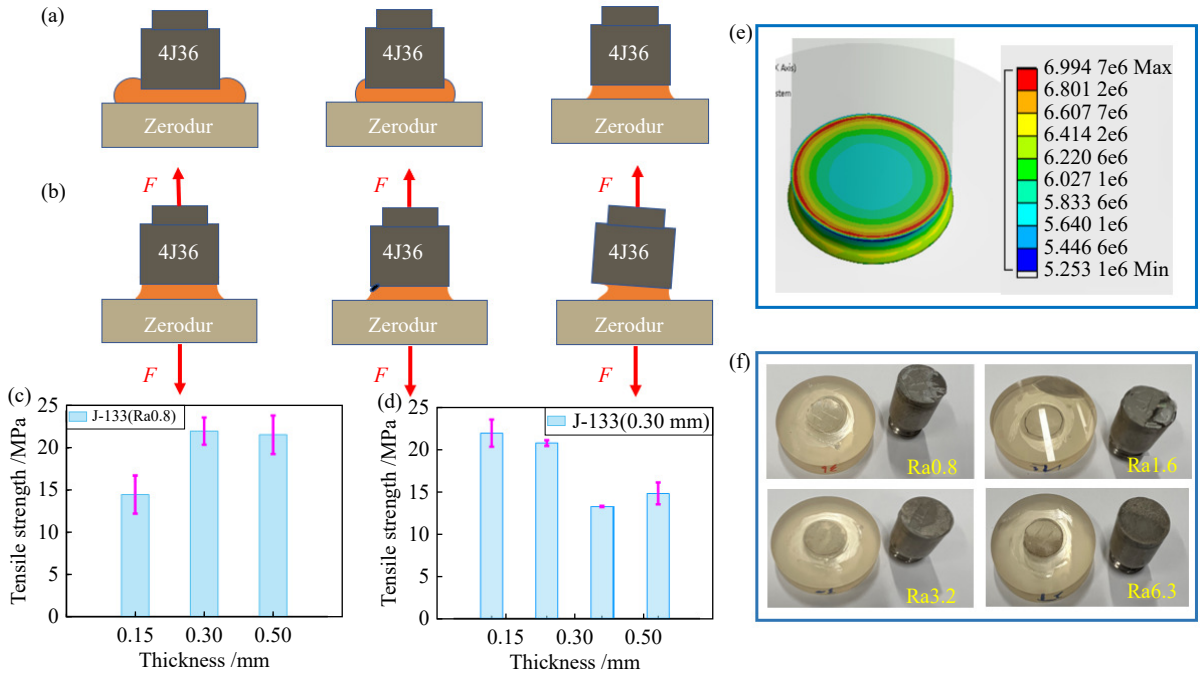

Fig. 6 Failure process and experimental results of J-133 bonding layer.

Figure 6(a) shows the evolution of the bonding-layer edges during the bonding process. Initially, the adhesive exhibited significant flow characteristics, forming a large semicircular structure at the edge under the influence of surface tension. To optimize the mechanical performance of the edge-bonding layer during solidification, the excess solution must be removed, resulting in the second edge structure shown in Fig. 6. Over time, as the bonding layer solidifies and contracts, the edge transitions to the third structure, as shown in Fig. 6(a). During tensile testing of the cured structure, cracks gradually formed at the bonding layer edges owing to the localized stress concentration, progressively enlarging, and eventually causing bonding-layer failure, as shown in Fig. 6(b). Figures 6(c) and 6(d) present the tensile performance statistics of the J-133 bonding layer at different thicknesses and substrate roughness levels. The failure cross-section revealed that the bonding-layer failure initiated from the edges and varied with the substrate surface roughness, which is consistent with the results of the finite element analysis, as shown in Fig. 6(e). When the substrate surface roughness was excessive, com-

plete detachment of the bonding layer occurred, as shown in Fig. 6(f). Therefore, from the perspective of bonding-layer failure, improving the surface quality of the Invar steel component is crucial during the integrated structural bonding process.

5 Conclusion

This study focuses on the structural design and experimental research of the integrated structure of the space gravitational-wave detector. First, the optimization design of the integrated structure was completed, and based on this, experimental research on the bonding layer connection was conducted. Then, with the aid of finite element analysis, the stress distribution of the bonding layer in the integrated structure under random vibration was analyzed. Experimental investigations were conducted on the tensile strength and failure modes of the three adhesives and their bonding processes. The experimental results demonstrated that J-133 exhibits optimal mechanical performance at a thickness of 0.30 mm and substrate surface roughness of Ra 0.8. The cross-sections after failure confirmed the occurrence of tearing and delamination in the tensile tests, indicating the susceptibility to stress concentration effects.

Copyright

References:

[1] KAWAMURA S, NAKAMURA T, ANDO M, *et al*.. Space gravitational-wave antennas DECIGO and B-DECIGO[J]. *International Journal of Modern Physics D*, 2019, 28(12): 1845001.

[2] TORRES-ORJUELA A, HUANG SH J, LIANG ZH CH, *et al*. . Detection of astrophysical gravitational wave sources by TianQin and LISA[J]. *Science China Physics*, *Mechanics & Astronomy*, 2024, 67(5): 259511.

[3] WANG H T, JIANG ZH, SESANA A, *et al*.. Science with the TianQin observatory: preliminary results on massive black hole binaries[J]. *Physical Review D*, 2019, 100(4): 043003.

[4] FAN Z C, ZHAO L J, CAO SH Y, *et al*.. High performance telescope system design for the TianQin project[J]. *Classical and Quantum Gravity*, 2022, 39(19): 195017.

[5] LIVAS J C, SANKAR S R. Optical telescope system-level design considerations for a space-based gravitational wave mission[J]. *Proceedings of SPIE*, 2016, 9904: 99041K.

[6] YU M, LI J C, LIN H G, *et al*.. Optical system design of large-aperture space gravitational wave telescope[J]. *Optical Engineering*, 2023, 62(6): 065107.

[7] ZHANG S, ZHAO D L. *Aerospace Materials Handbook*[M]. Boca Raton: CRC Press, 2012: 781.

[8] SANJUÁN J, PRESTON A, KORYTOV D, *et al*.. Carbon fiber reinforced polymer dimensional stability investigations for use on the laser interferometer space antenna mission telescope[J]. *Review of Scientific Instruments*, 2011, 82: 124501.

[9] CHWALLA M, DANZMANN K, ÁLVAREZ M D, *et al*.. Optical suppression of tilt-to-length coupling in the LISA long-arm interferometer[J]. *Physical Review Applied*, 2020, 14(1): 014030.

[10] LIGHTSEY P A, ATKINSON C, CLAMPIN M, *et al*.. James Webb Space Telescope: large deployable cryogenic telescope in space[J]. *Optical Engineering*, 2012, 51(1): 011003.

[11] HU H F, ZHOU D, ZHAO CH CH, *et al*.. Hetero-bonding strength investigation into opto-mechanical interface[J]. *Frontiers in Astronomy and Space Sciences*, 2024, 11: 1406090.

[12] ELLIFFE E J, BOGENSTAHL J, DESHPANDE A, *et al*.. Hydroxide-catalysis bonding for stable optical systems for space[J]. *Classical and Quantum Gravity*, 2005, 22(10): S257-S267.

[13] MASSO REID M, HAUGHIAN K, CUMMING A V, *et al*.. Temperature dependence of the thermal conductivity of hydroxide catalysis bonds between silicon substrates[J]. *Classical and Quantum Gravity*, 2023, 40(24): 245006.

[14] FAULKS H, GEHBAUER K, BISI M. LISA final technical report[C]. *Proceedings of the National Aeronautics and Space Administration*, 2000. **(查阅网上资料, 未找到本条文献信息, 请确认)**.

[15] AGARWAL P, KUMAR M, CHOUDHARY M, *et al*.. Experimental and numerical analysis of mechanical, thermal and thermomechanical properties of hybrid glass/metal fiber reinforced epoxy composites[J]. *Fibers and Polymers*, 2022, 23(5): 1342-1365.

[16] LI SH H, HU K J, HUI W CH, *et al*.. Shear strength and interfacial characterization of borosilicate glass-to-metal seals[J]. *Journal of Alloys and Compounds*, 2020, 827: 154275.

[17] WANG H R. Research on a bimorph piezoelectric deformable mirror for adaptive optics in optical telescope[J]. *Optics Express*, 2017, 25(7): 8115-8122.

[18] LI SH H, CAI Y Y, ZHU Q Y, *et al*.. Interface degradation of glass-to-metal seals during thermo-oxidative aging[J]. *Corrosion Science*, 2022, 199: 110189.

[19] LANCKER B V, CORTE W D, BELIS J. Investigation of the structural performance of continuous adhesive glass-metal connections using structural silicone and hybrid polymer adhesives[J]. *Engineering Structures*, 2024, 304: 117612.

[20] WANG W, XIAO Y Y, WU X Y, *et al*.. Optimization of laser-assisted glass frit bonding process by response surface methodology[J]. *Optics & Laser Technology*, 2016, 77: 111-115.

[21] RICHET P. *Encyclopedia of Glass Science, Technology, History, and Culture*[M]. Hoboken, New Jersey: Wiley: American Ceramic Society, 2021: 629-638.

Author Biographics：

ZHAO Hongchao (1985—), PH.D, Associate Professor, School of Advanced Manufacturing, Shenzhen Campus of Sun Yat-sen University. His research interests are in precision optical systems and ultra -precision and ultra-stable structures. E-mail: zhaohongch@mail.sysu.edu.cn

CHEN Wenduo (1986—), PH.D, Associate Professor, School of Materials, Shenzhen Campus of Sun Yat-sen University. Her research interests are in the computational simulation and big data work of polymer and composite materials. E-mail: chenwd29@mail.sysu.edu.cn